2104 J. Med. Chem. 2010, 53, 2104–2113
DOI: 10.1021/jm9016043

Journal of Medicinal Chemistry Article

Synthesis and Uptake of Fluorescence-Labeled Combi-molecules by P-Glycoprotein-Proficient and -Deficient Uterine Sarcoma Cells MES-SA and MES-SA/DX5

Anne-Laure Larroque-Lombard,[†,§] Margarita Todorova,[†,§] Nahid Golabi,[†] Christopher Williams,[‡] and Bertrand J. Jean-Claude*[,†]

[†]*Cancer Drug Research Laboratory, Department of Medicine, Division of Medical Oncology, McGill University Health Center/Royal Victoria Hospital, 687 Pine Avenue West Room M-719, Montreal, Quebec, H3A 1A1 Canada, and* [‡]*Chemical Computing Group Inc., 1010 Sherbrooke Street West, Suite 910, Montreal, Quebec H3A 2R7, Canada.* [§]*The two authors contributed equally to this paper.*

Received October 30, 2009

Here, we report on the first synthesis of fluorescent-labeled epidermal growth factor receptor−DNA targeting combi-molecules, and we studied the influence of P-glycoprotein status of human sarcoma MES-SA cells on their growth inhibitory effect and cellular uptake. The results showed that **6**, bearing a longer spacer between the quinazoline ring and the dansyl group, was more stable and more cytotoxic than **4**. In contrast to the latter, it induced significant levels of DNA damage in human tumor cells. Moreover, in contrast to doxorubicin, a drug known to be actively effluxed by P-gp, the more stable combi-molecule **6** induced almost identical levels of drug uptake and DNA damage in P-gp-proficient and -deficient cells. Likewise, in contrast to doxorubicin, **4** and **6** exerted equal levels of antiproliferative activity against the two cell types. The results *in toto* suggest that despite their size, the antiproliferative effects of **4** and **6** were independent of P-gp status of the cells.

Introduction

At the advanced stages, solid tumors express a variety of receptors and signaling proteins that not only drive their progression but also render them resistant to tumor drugs. One mechanism of multidrug resistance (MDR)[a] is the expression of a reflux pump [e.g., P-glycoprotein (P-gp)] that transports drugs out of the cells,[1−5] and this is responsible for drug resistance and treatment failure in approximately 90% of cancer patients.[6,7] Also, some mutations in key signaling proteins are often responsible for chemoresistance. Several attempts to modulate MDR led to a limited degree of success in the clinic, and the design of agents that diffuse into the cells regardless of their P-gp status or that selectively kill P-gp-expressing cells[8] has become a new drug development strategy.

Recently, to circumvent problems associated with target heterogeneity in advanced cancers, we developed novel types of drugs capable of inhibiting refractory tumor cell growth by blocking divergent targets such as the epidermal growth factor receptor (EGFR) and genomic DNA. Many prototypes of these agents termed combi-molecules have been shown to block the growth of human cancer cells with disordered signaling.[9−14] While their ability to concomitantly damage DNA and to induce high levels of apoptosis was demonstrated, the influence of transport pump-mediated MDR on the potency of these multitargeted molecules has yet to be explored. To analyze their intracellular uptake and dependence on MDR status, we designed fluorescence-labeled prototypes **4** (AL194) and **6** (AL237)[15] and studied their differential uptake by two human uterine sarcoma cell lines (MES-SA and MES-SA/DX5) that do not express EGFR,[16] the primary target of these combi-molecules. The use of cells deprived of EGFR was to avoid any interference of EGFR or related proteins with the retention or subcellular distribution of the molecules. We have now shown elsewhere that EGFR expression influences their subcellular distribution.[15] Importantly, in contrast to the parental MES-SA cell line, the MES-SA/DX5 has been shown to express P-gp and to be resistant to doxorubicin and paclitaxel.[17−19]

The new combi-molecules reported herein were designed to degrade into an aminoquinazoline, fluorescing in the blue, and a dansylated DNA-damaging moiety, fluorescing in the green, thereby facilitating the analysis of drug uptake by fluorescence microscopy and flow cytometry. The IC_{50} values for EGFR tyrosine kinase inhibition by **4** and **6** were 1.4 and 0.6 μM, respectively, and their binary EGFR−DNA targeting properties are extensively discussed in a separate report.[15]

Here, we describe the synthesis of the two combi-molecules, one with a short neutral ethano linker and the other with a longer and basic *N*-methylethanediamine spacer. We compared their differential uptake in MES-SA cells with that of doxorubicin, by fluorescence microscopy and flow cytometry. In contrast to the clinical anticancer drug doxorubicin, the potency of these bulky molecules was independent of the P-gp status of the two cell types. It should be noted that the purpose of this study was not to compare the potency of the fluorescent molecules with that of doxorubicin, a strong DNA intercalator and topoisomerase II inhibitor, but was rather to analyze their differential uptake in comparison with that of doxorubicin, a highly P-gp-dependent drug.

Results and Discussion

Chemistry. The synthesis of compound **4** and **6** proceeded according to Schemes 1 and 2, respectively. Commercially

*To whom correspondence should be addressed. Tel: 514-934-1934 ext 35841. Fax: 514-843-1475. E-mail: jacques.jeanclaude@staff.mcgill.ca.

[a]Abbreviations: P-gp, P-glycoprotein; EGFR, epidermal growth factor receptor; MDR, multidrug resistance.

 Published on Web 02/12/2010

Scheme 1. Synthesis of Compound **4**[a]

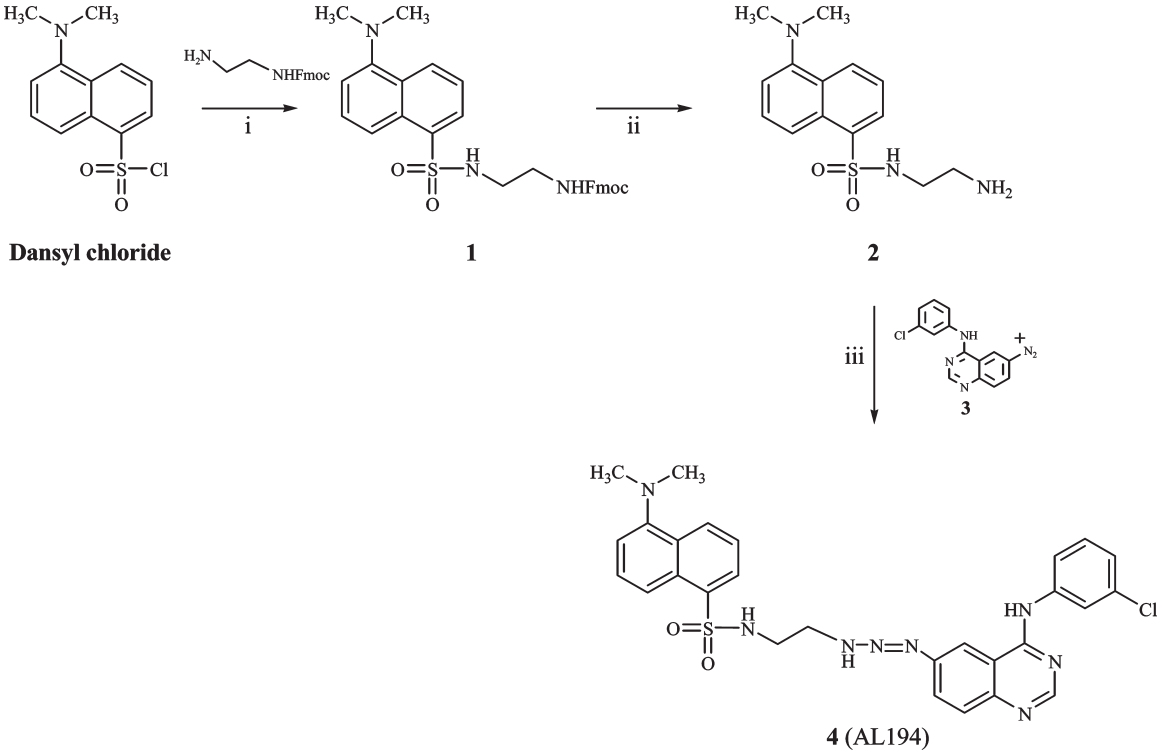

[a] Reagents and conditions: (i) *N*-Fmoc-ethylenediamine, EtOAc, H_2O, K_2CO_3, 0 °C. (ii) Morpholine, DMF, room temperature. (iii) Diazonium **3**, Et_3N, CH_3CN/Et_2O, −5 °C.

Scheme 2. Synthesis of Compound **6**[a]

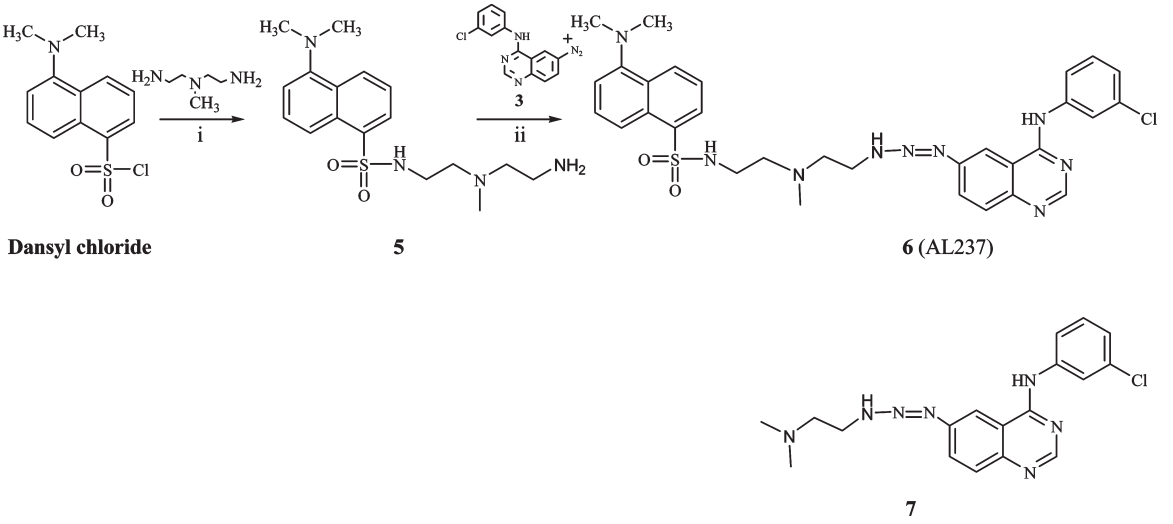

[a] Reagents and conditions: (i) *N*-(2-Aminoethyl)-*N*-methylethanediamine, EtOAc, 0 °C. (ii) Diazonium **3**, Et_3N, CH_3CN/Et_2O, −5 °C.

available 9-fluorenylmethyl *N*-(2-aminoethyl)carbamate hydrochloride was treated with dansyl chloride in a biphasic ethyl acetate/aqueous potassium carbonate solution to give **1** (Scheme 1). Compound **1** was deprotected with morpholine in DMF to give the amino compound **2**. In parallel, the aminoquinazoline was diazotized in dry acetonitrile with nitrosonium tetrafluoroborate to provide the diazonium salt **3** as previously described.[14] Diazonium salt **3** was coupled with **2** in the presence of triethylamine *in situ* to give the desired compound **4**. Several attempts to purify **4** by column chromatography failed due to on-column degradation, which we believe could be due to the conversion of **4** to a product resulting from loss of nitrogen. Successful purification was achieved by serial trituration of compound **4** with methylene chloride, ether, and petroleum ether to give a pure red-brown powder. The compound was characterized by NMR and MS, and its purity was confirmed by elemental analysis.

The synthesis of compound **6** proceeded in a similar fashion. An excess of commercially available *N*-(2-aminoethyl)-*N*-methylethanediamine was treated with dansyl chloride to give **5** in ethyl acetate at 0 °C (Scheme 2), and this

Table 1. Half-Lives of Compounds **4** and **6** in a Serum-Containing Medium

Compound	4	6
t ½ (min)	4.96 ± 0.04*	21.72 ± 0.27*
	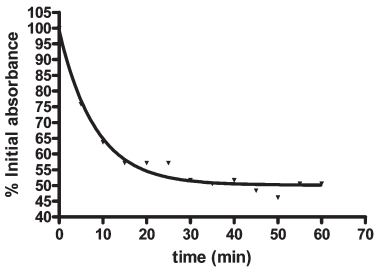	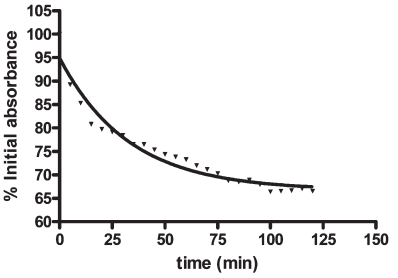

* Data are means of three experiments in triplicate.

product was coupled with the diazonium salt of quinazoline **3** to give **6**. The purification of **6** was as difficult as that of **4**. All attempts to purify this compound by column chromatography failed. Serial trituration provided a pure red-brown powder that was analytically pure. The structure of **6** was further confirmed by NMR and MS.

Half-Life in a Serum-Containing Medium. The sole structural difference between **4** and **6** is in the nature of the linker. The linker in **4** is an ethylene group between the sulfonamido moiety of the dansyl and the N3 of the triazene, leaving no possibility for intramolecular hydrogen bonding. By contrast, the dansyl in **6** is separated by six bond lengths and contains a methylamino group three bond lengths away from the N3 of the triazene, leaving the possibility for intramolecular hydrogen bonding. Interestingly, **4** was 5-fold less stable than **6** with a half-life as short as 5 min (Table 1). Perhaps, the intramolecular interaction between the *N*-methylamino group and the triazene plays a significant stabilizing role. We have already evoked a similar interaction for explaining the stability of **7** (Scheme 2), a stable dimethyaminoethyl triazene with a $t_{1/2}$ = 108 min[10] that showed significant antitumor activity *in vivo*.[20] To further elaborate on the importance of the *N*-methylamino group on the stability of **6**, we undertook a molecular modeling study using AM1 semi-empirical calculation.

As outlined in Figure 1, conformer **1** containing a H-bond is computed to be ~2 kcal/mol more stable than conformer **2**, which lacks the H-bond. Conformer **1** has the proposed H-bond (2.62 Å distance) that stabilizes it. The H-bond is absent in conformer **2**, as the hydrogen and the amine nitrogen are *trans* to one another at a distance of 4.08 Å. Compound **4**, which is not able to adopt H-bond-stabilizing conformations, is less stable. However, in aqueous solution, the superior stability of **6** is better rationalized in terms of the equilibria depicted in Schemes 3 and 4. Because the central nitrogen in **6** is protonated at physiological pH, the transition state to the formation of the doubly charged species **F** should have a higher energy when compared with that for **C** in Scheme 4. This may account for the slower rate of hydrolysis for **6** when compared with **4** under physiological conditions.

Differential Growth Inhibitory Activity. The potency of the two dansylated compounds was compared in MES-SA cells

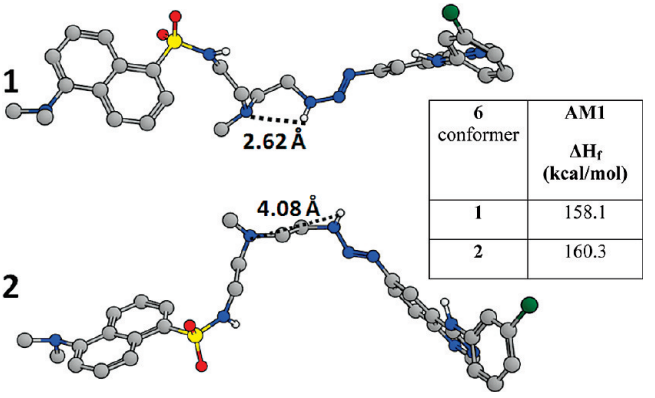

6 conformer	AM1 ΔH_f (kcal/mol)
1	158.1
2	160.3

Figure 1. Molecular modeling using AM1 semi-empirical calculation of **6**. The H−N distances are given in Å.

that do not express P-gp. MES-SA cells are also deprived of EGFR expression.[16] Therefore, the EGFR inhibitory activity of the quinazoline side chain would not influence the growth inhibitory effect of compounds **4** and **6**. The results showed that **6** was 3-fold more potent than **4** (Figure 2A). Perhaps the rapid decomposition of **4** compromised its optimal cellular delivery. We also observed a 2-fold stronger potency for **6** in the MDA-MB-468 breast cancer cells that express EGFR but do not express P-gp,[21,22] indicating that **6** was more potent than **4** regardless of the P-gp and the EGFR status of the cells (Figure 2B).

Because our primary goal was to compare the cellular penetration of the two compounds in P-gp-proficient and -deficient cells, we tested their effects on both MES-SA (P-gp-deficient) and its derived MES-SA/DX5 (P-gp-proficient) cells. The latter cell line expresses high levels of P-gp and is resistant to doxorubicin. Using the SRB assay, we showed a 20-fold difference between the sensitivity of MES-SA and MES-SA/DX5 to doxorubicin. In contrast, no significant difference ($P > 0.05$) was seen for both **4** and **6** in their potency against the two cell lines. Combi-molecule **6** was equally potent in both cell lines, and **4** was 1.6-fold more potent against MES-SA/DX5 than MES-SA, indicating an even greater potency in the cells that express P-gp.

Cellular Uptake. To verify whether the differential responses correlated with cell penetration, we exploited the

Scheme 3. Degradation Pathway of Compound **6** in Physiological Conditions

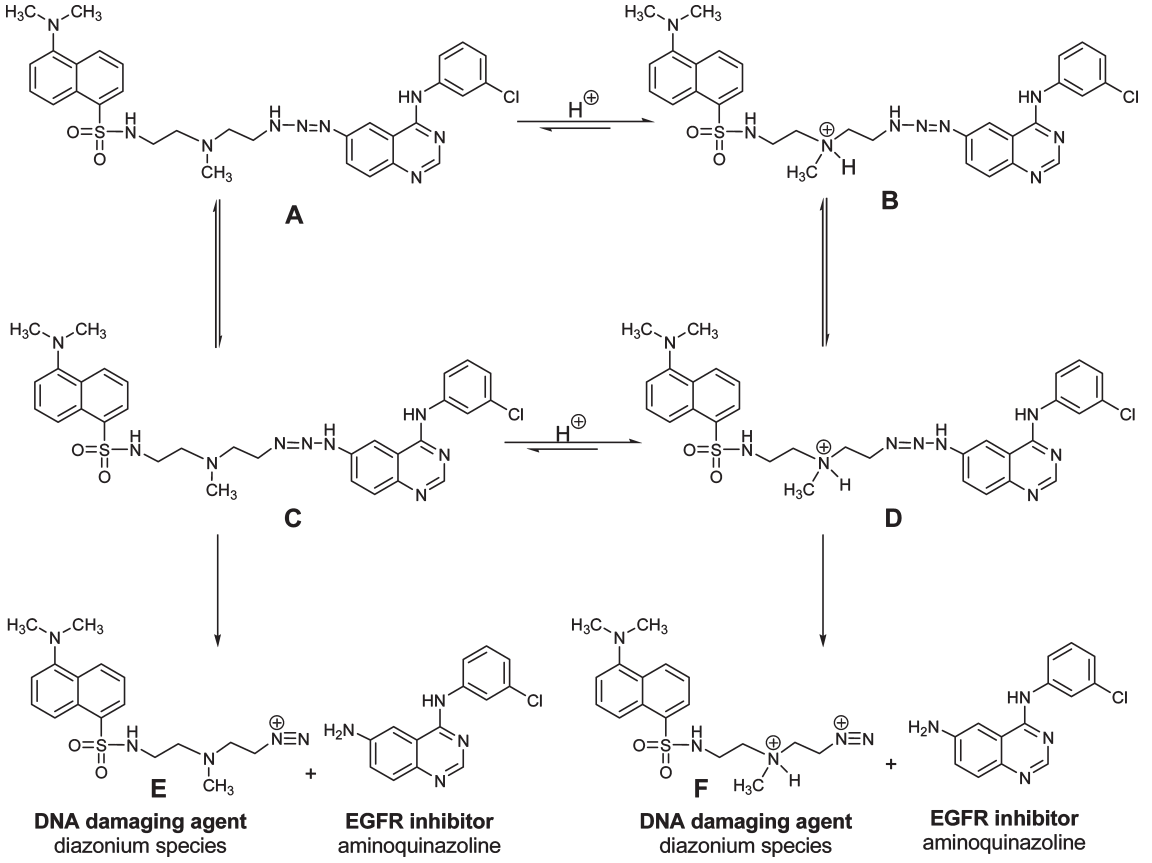

Scheme 4. Degradation Pathway of Compound **4** in Physiological Conditions

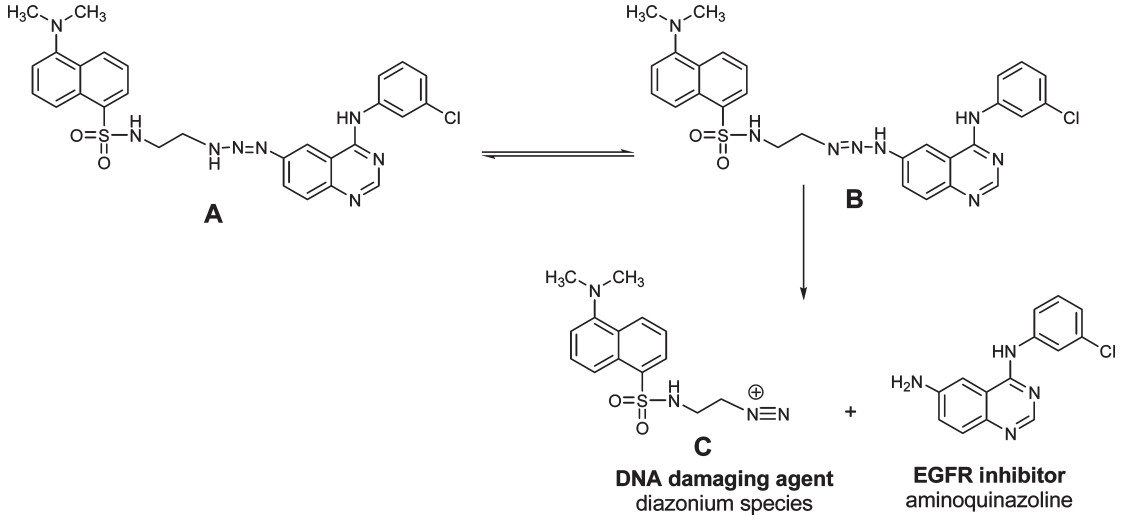

fluorescent properties of doxorubicin and those of compounds **4** and **6** to analyze their intracellular content by fluorescence microscopy and flow cytometry. We have previously used flow cytometry to analyze doxorubicin and compound **6** internalization in human breast tumor cells.[15,23]

Fluorescence microscopy in the parental cell line showed a homogeneous distribution of doxorubicin (Figure 3A, upper panel) throughout the cell population. By contrast, in the MES-SA/DX5 cells (Figure 3A, lower panel), the distribution was heterogeneous with a fraction of the cell population emitting high fluorescence and another with poor to no internalization of doxorubicin. As shown in Figure 4A, **4** and **6** penetrate the cells and decompose inside the cells to generate its bioactive species: EGFR inhibitor, blue fluorescence, and a DNA-damaging species, green fluorescence. The two colors were observed at similar intensity in both cell types. Flow cytometric analysis permitted the quantification of the proportion of cells that did not internalize doxorubicin (Figure 3B) and the combi-molecules (Figure 4B). For the more potent compound **6**, at a dose range starting with the IC_{50} for growth inhibition, no differential internalization between the two cell types was seen. In contrast, 40% of the

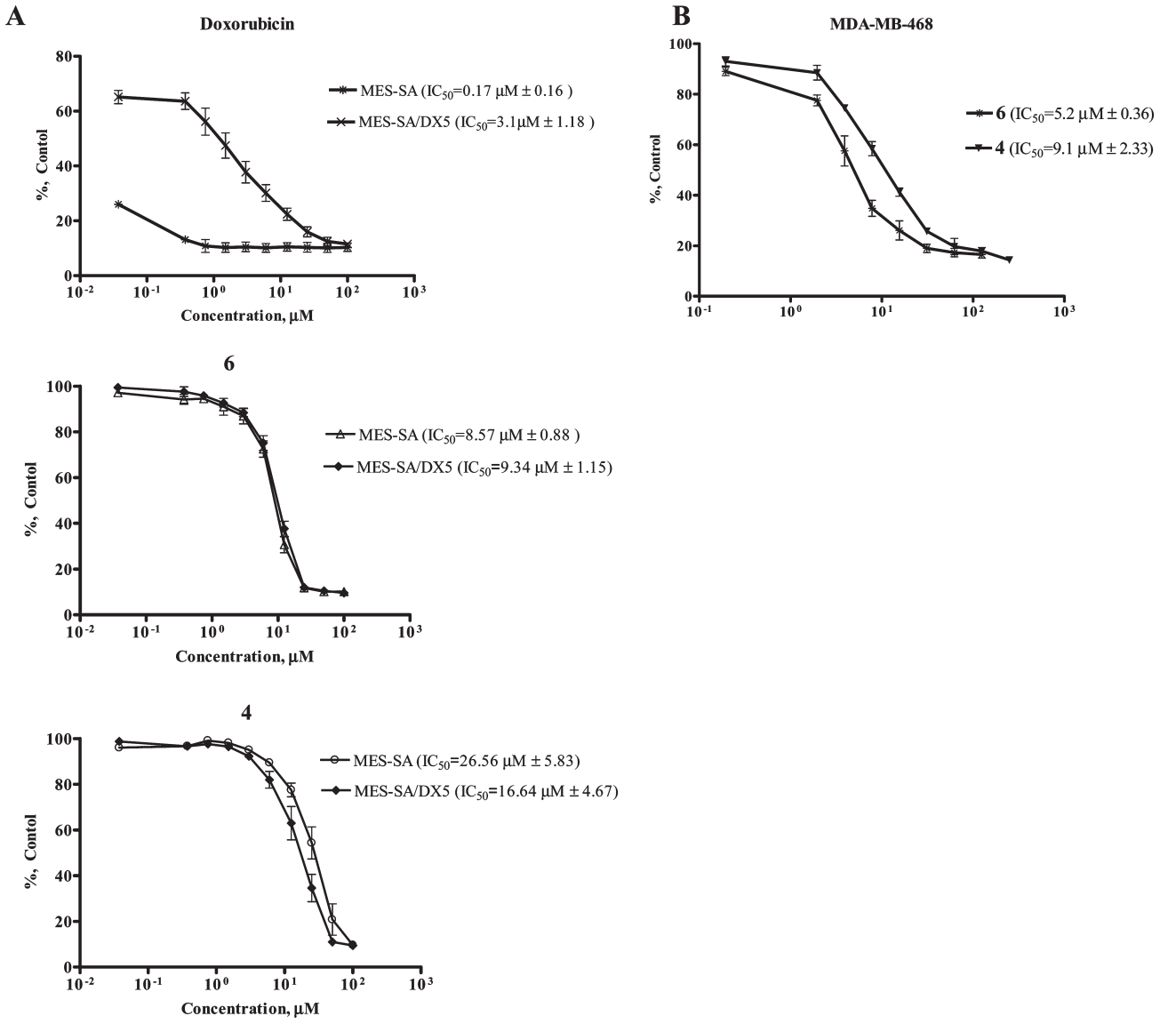

Figure 2. Growth inhibition of doxorubicin, **4**, and **6** by SRB assay. (A) Comparison of antiproliferative activity of doxorubicin, **4**, or **6** in MES-SA and MES-SA/DX5 cells after 96 h. (B) Growth inhibition of **4** and **6** in human breast MDA-MB-468 cells. Each point represents an average of two independent experiments performed in triplicate.

cell population could not internalize doxorubicin at this dose range.

DNA Damage. The DNA-damaging property of compounds **4** and **6** was assessed by alkaline comet assay. The visualization of DNA comet tails in both cell lines using fluorescence microscopy showed that **6** was a strong DNA-damaging agent, while **4** was not able to induce DNA damage (Figure 5). This result is consistent with the stability of the two molecules and also that of the putative dansylated alkyldiazonium released after degradation. The rapid decomposition of **4** seems again to limit its activity. Moreover, **6** damaged DNA in both cell lines with the same intensity, independently of P-gp status, which is in agreement with the growth inhibitory results, and also indicated that the combimolecule can penetrate and decompose inside the cells to deliver the DNA-damaging moiety (green fluorescence, Figure 4A). The levels of DNA damage induced by doxorubicin were also analyzed in the two cell types, and a differential response was seen with doxorubicin inducing a 2-fold greater number of DNA-damaged cells in the MES-SA population when compared with MES-SA/DX5 (Figure 3C). Cells with a higher comet tail moment than the control were scored as damaged, and the data were presented as percent of cells with damaged DNA. This result was consistent with the differential level of doxorubicin uptake observed between these two cell types.

Conclusion

At the advanced stages of many cancers, drug transport is significantly affected by several mechanisms including P-gp-mediated drug efflux.[1−5] This presents a daunting challenge to drug development against advanced cancers. The combimolecules are designed to possess multiple targeting properties with the purpose of simultaneously blocking several signaling networks in the cells. To this end, several pharmacophores must be appended to one single core structure. Therefore, this leads to the branching of pharmacophores through bulky linkers that often affect the size of the resulting molecules and, as a result, their transport into the cells. It is now well-known that the greater the size of an agent is, the

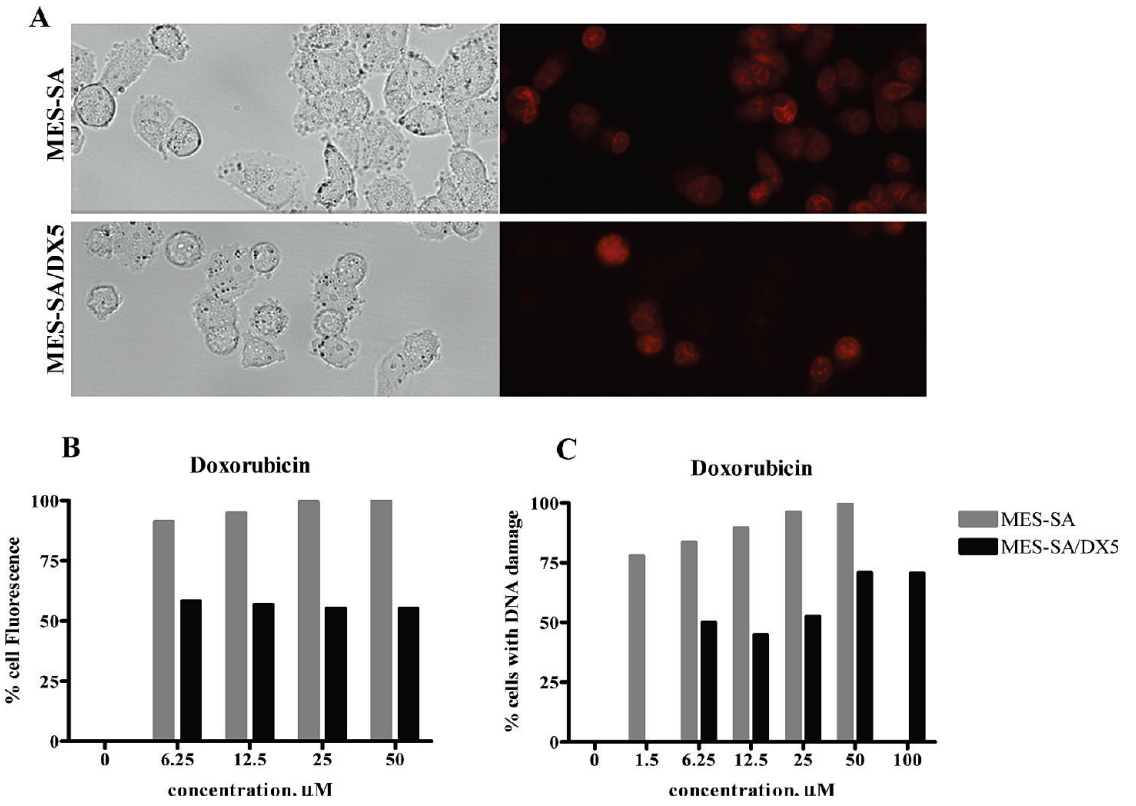

Figure 3. Cellular fluorescence and DNA damage by doxorubicin. (A) Intracellular accumulation of doxorubicin in P-gp-positive and -negative cells was determined by fluorescence microscopy. Cells were incubated with 25 μM doxorubicin for 2 h and washed with PBS, and fluorescence was visualized with a Leica fluorescent microscope (40× magnification). (B) Cellular fluorescence of doxorubicin by FACS. The levels of accumulated fluorescence for doxorubicin (0, 6.25, 12.5, 25, and 50 μM) were quantified in MES-SA and MES-SA/DX5 cells after 2 h. (C) DNA damage induced by doxorubicin in MES-SA (0, 1.5, 6.25, 12.5, 25, and 50 μM) and MES-SA/DX5 (0, 6.25, 12.5, 25, 50, and 100 μM) cells. Cells were exposed for 2 h to doxorubicin, and DNA damage was measured using an alkaline comet assay. Fifty cells were scored from each dose, and the comet tail moment was calculated by comet IV software (Perceptive Instruments). Cells with a comet tail moment greater than that in the control were scored positive and expressed as percent of cells with damaged DNA.

more likely that its transport mechanism across the cell membrane will be influenced by efflux proteins. Here, we discovered that at least one mechanism of drug efflux may not prevent cell penetration by two prototypical combi-molecules designed to block EGFR−DNA and carrying a bulky fluorescence-labeled moiety. Although the molecular mechanism of such an important observation requires further elucidation, we believe that the fact that the combi-molecules are designed to decompose inside the cells to generate their bioactive species might be a mean by which the rapid efflux of the intact structure was impeded.

Experimental Section

Chemistry. ^{1}H NMR spectra and ^{13}C NMR spectra were recorded on a Varian 300 MHz spectrometer. Chemical shifts are given as δ values in parts per million (ppm) and are referenced to the residual solvent proton or carbon peak. Mass spectrometry was performed by the McGill University Mass Spectroscopy Center, and electrospray ionization (ESI) spectra were performed on a Finnigan LC QDUO spectrometer. Data are reported as m/z (intensity relative to base peak = 100). Elemental analyses were carried out by GCL & Chemisar Laboratories (Guelph, Ontario, Canada). The analyses were done two times. All chemicals were purchased from Sigma-Aldrich. Dansyl chloride was purchased from Alfa Aesar, *N*-(2-aminoethyl)-*N*-methylethanediamine was from Wako Pure Chemical Industries, Ltd., and mono-Fmoc-ethylenediamine hydrochloride was from Novabiochem. The purities of all compounds tested were > 95% as determined by elemental analysis.

Compound 1, 2-Dansyl-9-fluorenylmethyl *N*-(2-Aminoethyl)-carbamate. 9-Fluorenylmethyl *N*-(2-aminoethyl)carbamate hydrochloride (500 mg, 1.57 mmol) was dissolved in water saturated with potassium carbonate and ethyl acetate (50 mL/50 mL). The mixture was cooled to 0 °C, and a solution of dansyl chloride (3 equiv) in ethyl acetate was added dropwise. The reaction mixture was stirred, and the temperature was raised to room temperature. After 4 h, the organic layer was separated, washed with brine twice and dried with magnesium sulfate, filtered, and evaporated to provide a yellow-green oil, which was purified by trituration in ethyl ether. A white pure solid of compound **1** was obtained after filtration (742 mg, 92%). ^{1}H NMR (300 MHz, DMSO-d_6): δ ppm 2.75 (m, 2H), 2.80 (s, 6H), 2.95 (m, 2H), 4.21 (m, 3H), 7.25 (m, 4H), 7.37 (m, 2H), 7.59 (m, 4H), 7.85 (d, J =7.5 Hz, 1H), 7.99 (m, 1H), 8.08 (d, J =7.5 Hz, 1H), 8.24 (d, J =8.1 Hz, 1H), 8.45 (d, J =8.7 Hz, 1H).

Compound 2, Dansyl-*N*-(2-aminoethyl)amide. The Fmoc group was removed with morpholine/DMF 1/1 (2 mL) for 30 min at room temperature. The reaction mixture was evaporated, and the crude product was extracted with ethyl acetate and acidic water phase (pH 2). The aqueous phase was alkalinized to pH 5 and extracted with ethyl acetate to eliminate the secondary products from the aqueous layer. The pH was increased to 10, and this aqueous layer was extracted again with ethyl acetate. The organic layer was dried, and the magnesium sulfate was filtered and evaporated to provide pure free amine **2** (148 mg, 87%). ^{1}H NMR (300 MHz, DMSO-d_6): δ ppm 2.45 (m, 2H), 2.75 (m, 2H), 2.81 (s, 6H), 7.24 (d, J =7.2 Hz, 1H), 7.59 (q, J =7.5 Hz, 2H), 8.09 (d, J =7.2 Hz, 1H), 8.28 (d, J =8.4 Hz, 1H), 8.45 (d, J =8.7 Hz, 1H).

Compound 5, Dansyl-*N*-(2-[(2-aminoethyl)-*N*-methylamino]ethyl)-amide. Dansyl chloride (1 g, 3.71 mmol) was dissolved in 20 mL

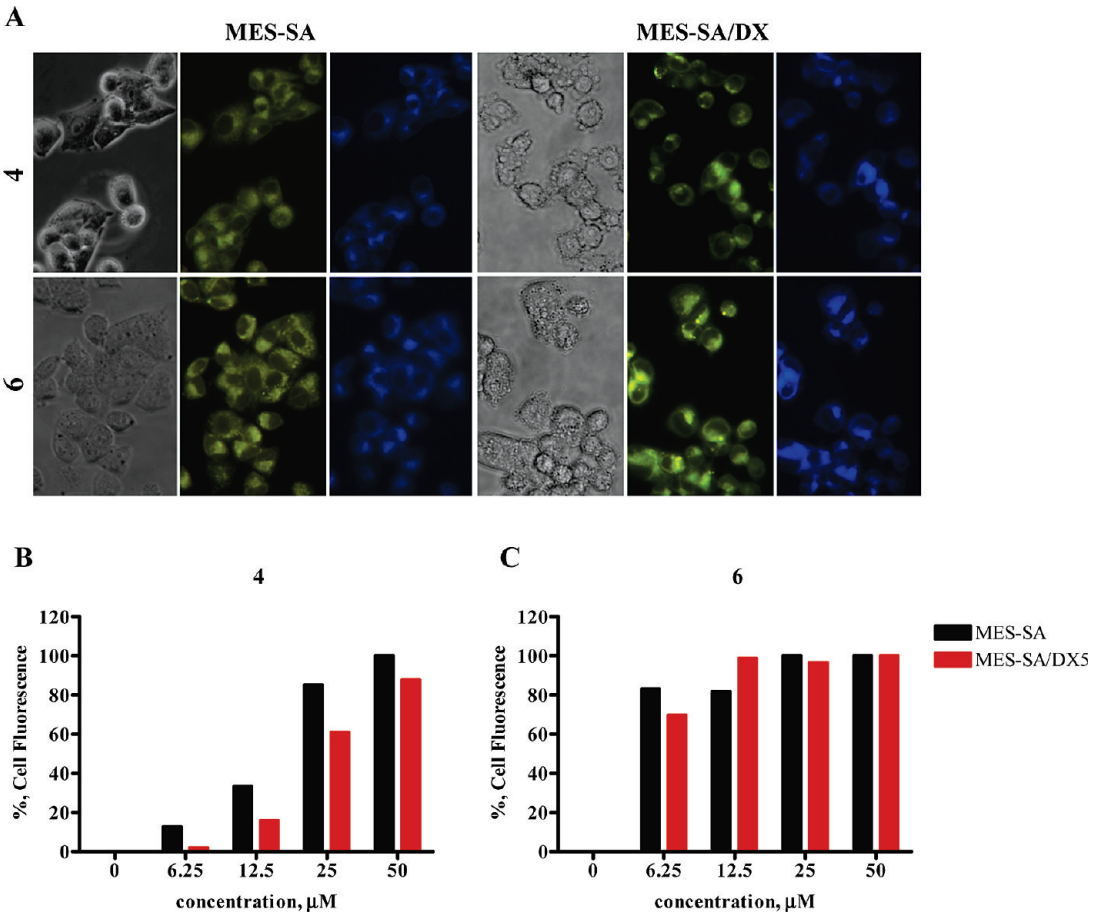

Figure 4. (A) Cellular fluorescence of **4** and **6** by fluorescence microscopy. MES-SA and MES-SA/DX5 cells were incubated with **4** and **6** for 2 h, and imaging was performed with Leica fluorescent microscope (40× magnification). Visualization of **4** and **6** degradation species: Blue aminoquinazoline and green dansylated species were imaged using individual filters. (B) Cellular fluorescence of **4** and **6** by FACS. The levels of accumulated fluorescence for **4** and **6** (0, 6.25, 12.5, 25, and 50 μM) were quantified in MES-SA and MES-SA/DX5 cells by FACS, and results were analyzed with GraphPad Prism software.

of ethyl acetate and was added dropwise to a cold solution of *N*-(2-aminoethyl)-*N*-methylethanediamine (2.38 mL, 5 equiv) in 80 mL of ethyl acetate. The reaction mixture was stirred at 0 °C under argon. After 2 h, the solution was extracted with neutral water and acidic water (pH 2−3). This acidic water was alkalinized and was extracted with ethyl acetate two times. The organic layer was dried with magnesium sulfate, filtered, and evaporated to provide a yellow oil, which was purified by crystallization in a minimum of ethyl acetate. White pure crystals of compound **5** were obtained (1.117 g, 86%). ^{1}H NMR (300 MHz, DMSO-d_6): δ ppm 1.92 (s, 3H), 2.13 (t, J = 6.3 Hz, 2H), 2.21 (t, J = 6.7 Hz, 2H), 2.40 (t, J = 6.1 Hz, 2H), 2.81 (s, 6H), 2.84 (t, J = 6.9 Hz, 2H), 7.21 (d, J =7.5 Hz, 1H), 7.58 (m, 2H), 8.11 (d, J = 7.2 Hz, 1H), 8.27 (d, J = 8.4 Hz, 1H), 8.43 (d, J = 8.1 Hz, 1H).

Compound 4. The diazonium compound **3** was synthesized as described in ref 14: Amino-anilinoquinazoline (50 mg, 0.184 mmol) was dissolved in dry acetonitrile (5 mL) under argon and cooled to −5 °C. Nitrosonium tetrafluoroborate (2 equiv) in acetonitrile was added directly. After 30 min at −5 °C, the resulting clear orange solution was added dropwise to another solution of compound **2** (1 equiv) in acetonitrile with triethylamine (2 equiv) at 0 °C, after which the mixture was extracted with ethyl acetate and brine. The organic layer was dried with potassium carbonate and evaporated to provide a brown residue, which was purified by serial trituration: First, the crude product was dissolved in a minimum of methylene chloride and precipitated with petroleum ether and after was triturated in ether/petroleum ether 1/4 to give after filtration a red-brown solid (93 mg, 88%). ^{1}H NMR (300 MHz, DMSO-d_6): δ ppm 2.77 (s, 6H), 3.10 (m, 2H), 3.59 (m, 2H), 7.13 (d, J = 8.4 Hz, 1H), 7.22 (d, J = 7.5 Hz, 1H), 7.39 (m, 1H), 7.59 (m, 2H), 7.73 (d, J = 8.7 Hz, 1H), 7.86 (m, 2H), 8.13 (m, 2H), 8.27 (d, J = 8.7 Hz, 1H), 8.35 (s, 1H), 8.43 (d, J = 9.0 Hz, 1H), 8.58 (s, 1H), 9.89 (s, 1H), 10.59 (m, 1H). ^{13}C NMR (75 MHz, DMSO-d_6): δ ppm 158.13, 153.92, 152.05, 149.23, 148.90, 141.70, 136.29, 133.36, 130.71, 130.23, 129.74, 129.70, 129.50, 129.08, 128.61, 125.68, 124.28, 123.58, 121.89, 120.84, 119.71, 116.28, 115.82, 115.18, 51.72, 46.31, 45.72 (2C). ESI m/z 572.9 (MH^+ with ^{35}Cl). Anal. ($C_{28}H_{27}ClN_8O_2S$) C, H, N.

Compound 6. The diazonium compound **3** was still synthesized as previously described.[14] Amino-anilinoquinazoline (608 mg, 2.246 mmol) was dissolved in dry acetonitrile (80 mL) under argon and cooled to −5 °C. Nitrosonium tetrafluoroborate (2 equiv) in acetonitrile was added directly. After 30 min at −5 °C, the resulting clear solution was added dropwise to another solution of compound **5** (1 equiv) in acetonitrile with triethylamine (2 equiv) at 0 °C, after which the mixture was extracted with ethyl acetate and brine. The organic layer was dried with potassium carbonate and evaporated to provide a brown residue, which was purified by serial trituration. The crude product was dissolved in a minimum of methylene chloride and precipitated with petroleum ether, after which it was triturated in ether/petroleum ether 1/4 to give after filtration a red-brown solid (1.2 g, 85%). ^{1}H NMR (300 MHz, DMSO-d_6): δ ppm 1.99 (s, 3H), 2.32 (m, 2H), 2.52 (m, 2H), 2.77 (s, 6H), 2.90 (m, 2H), 3.53 (m, 2H), 7.12 to 7.21 (m, 2H), 7.39 (m, 1H), 7.55 (m, 2H), 7.75 to 7.97 (m, 4H), 8.12 (m, 2H), 8.30 (d, J = 8.4 Hz, 1H), 8.40

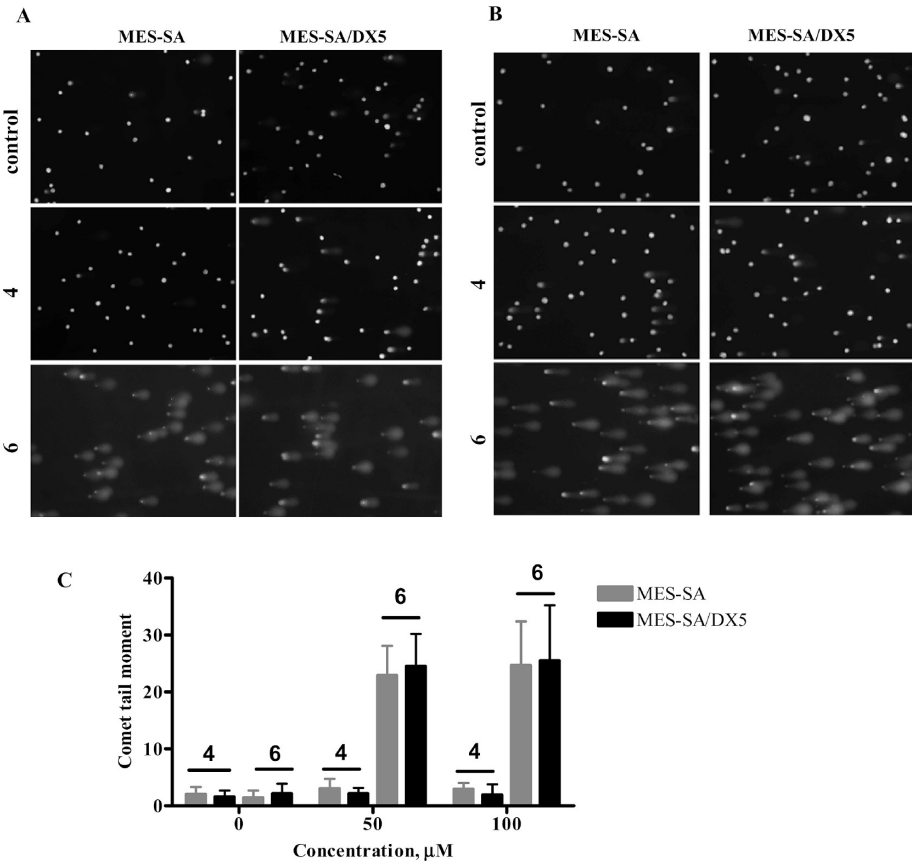

Figure 5. DNA damage induced by **4** and **6** at 50 (A) and 100 μM (B). MES-SA and MES-SA/DX5 cells were exposed to each combi-molecule for 2 h followed by assessment of drug-induced DNA damage using an alkaline comet assay. Visualization of DNA comets in both cell lines by fluorescence microscopy (10× magnification) after staining with SYBR Gold. (C) Fifty comets were scored, and the comet tail moment was quantified by comet IV software (Perceptive Instruments). Two independent experiments were averaged for each cell line, and data were analyzed with GraphPad Prism software.

(m, 1H), 8.43 (s, 1H), 8.60 (s, 1H). ^{13}C NMR (75 MHz, DMSO-d_6): δ ppm 158.10, 153.83, 152.01, 149.73, 148.78, 141.75, 136.69, 133.37, 130.72, 130.07, 129.76, 129.69, 129.56, 128.92, 128.54, 125.40, 124.25, 123.55, 121.83, 120.79, 119.77, 116.37, 115.76, 115.29, 57.04 (2C), 53.84, 46.40, 45.72 (2C), 41.51. ESI m/z 632.1 (MH^+ with ^{35}Cl). Anal. ($C_{31}H_{34}ClN_9O_2S$) C, H, N.

Half-Lives. The half-lives of **4** and **6** under physiological conditions were studied by UV spectrophotometer, Farmacia Biotech Ultrospec 2000. The compounds were dissolved in minimum volume of DMSO and diluted with DMEM supplemented with 10% FBS, and the absorbances were read at 335 nm for **4** and 350 nm for **6** in a quartz UV cell maintained at 37 °C with a circulating water bath. The experiment was repeated three times for each compound. The half-life was estimated by a one-phase exponential decay curve-fit method using the GraphPad software package (GraphPad software, Inc., San Diego, CA). The thermometer was Traceable VWR digital with ±0.005 °C accuracy.

Molecular Modeling. Molecular modeling was performed with MOE software (version 2006.08) available from Chemical Computing Group Inc. (Montreal, Quebec, Canada; www.chemcomp.com).

Biology. Cell Culture. All three cell lines were purchased from the American Type Culture Collection (ATCC, Manassas, VA). Human uterine sarcoma cells, MES-SA, and MES-SA/DX5 (ATCC: CRL-1976 and CRL-1977, respectively) were maintained in McCoy 5A medium, and human breast cancer cells MDA-MB-468 were cultured in DMEM. All media were supplemented with 10% FBS, 1.5 mM L-glutamine (Wisent Inc., St.-Bruno, Canada), and 100 μg/mL penicillin/streptomycin (GibcoBRL, Gaithersburg, MD). Cells were grown exponentially at 37 °C in a humidified atmosphere of 95% air and 5% carbon dioxide. In all assays, cells were plated 24 h before drug treatment.

Drug Treatment. Compounds **4** and **6** were synthesized in our laboratory, and doxorubicin hydrochloride was purchased from the hospital drug store (Mayne Pharma Inc., Montreal). In all assays, molecules were dissolved in DMSO (50 mM stock solution), and doxorubicin was dissolved in sterile water (2 mg/mL stock solution) and subsequently diluted in McCoy 5A medium before it was added to cells. The concentration of DMSO never exceeded 0.1% (v/v) during treatment.

Growth Inhibition Assay. MES-SA, MES-SA/DX5, and MDA-MB-468 cells were plated at a density of 5000 cells/well in 96-well flat-bottomed microtiter plates (100 μL of cell/well). Cells were allowed to attach overnight and then were treated with different drug concentrations for 96 h. Thereafter, cells were fixed using 50 μL of 50% trichloroacetic acid for 60 min at 4 °C, washed four times with water, stained with sulforhodamine B (SRB 0.4%) for 2 h at room temperature, rinsed four times with 1% acetic acid, and allowed to dry.[24] The resulting colored residue was dissolved in 200 μL of Tris base (10 mM, pH 10.0), and the optical density was recorded at a wavelength of 492 nm using a Bio-Rad microplate reader (model 2550). The results were analyzed by GraphPad Prism (GraphPad Software, Inc.), and the sigmoidal dose−response curve was used to determine 50% cell growth inhibitory concentration (IC_{50}). Each point represents the average of at least three independent experiments run in triplicate.

DNA Damage by Alkaline Comet Assay. The alkaline comet assay was performed as previously described.[25−27] Briefly, cells were exposed to doxorubicin (0, 1.5, 6.25, 12.5, 25, and 50 μM),

4, and **6** (0, 50, and 100 μM) for 2 h, harvested by trypsinization, collected in ice-cold PBS by centrifugation at 3000 rpm for 5 min, and then resuspended in PBS at 1×10^6 cells/mL. Cells were mixed with low melting point agarose (0.7%) in PBS at 37 °C (final dilution 1:10), followed by layering the agarose/cells suspension on GelBond film (Lonza, Rockland, ME). The agarose/cell suspension was allowed to solidify for 10 min and then immediately placed in lysis buffer [2.5 M NaCl, 100 mM tetra-sodium EDTA, 10 mM Tris-base, 1% (w/v) *N*-lauroylsarcosine, 10% (v/v) DMSO, and 1% (v/v) triton X-100, pH 10.0] overnight at 4 °C. Thereafter, the gels were rinsed with distilled water, equilibrated in alkaline electrophoresis buffer [300 mM NaOH, 10 mM tetra-sodium EDTA, 7 mM 8-hydroxyquinoline, 2% (v/v) DMSO, pH 13.0] for 30 min at room temperature, and electrophoresed at 20 V for 25 min in fresh eletrophoresis buffer. The gels were subsequently neutralized in 1 M ammonium acetate and then dehydrated in 100% ethanol overnight. Comets were visualized at 10× magnification using Leica fluorescent microscope after staining with SYBR Gold (1:10000, Molecular Probes, Eugene, OR) for 45 min.

Fluorescence Microscopy. Fluorescent properties of molecules were used to image drug transport efficiency and intracellular accumulation. MES-SA and MES-SA/DX5 cells were plated at 70% confluence in six-well plates, allowed to adhere overnight, and treated with 0, 25, and 50 μM **4**, **6**, or doxorubicin. After 2 h, cells were washed twice with PBS and were directly imaged at 40× using Leica fluorescent microscope (Leica DFC300FX camera) without fixation.

Flow Cytometry Analysis of Intracellular Drug Fluorescence. MES-SA and MES-SA/DX5 cells were plated at 0.5×10^6 cells per well in six-well plates, allowed to adhere overnight, and incubated in the presence of **4** and **6** or doxorubicin (0, 1.25, 6.25, 12.5, 25, and 50 μM) for 2 h. Cells were collected by trypsinization, washed twice with PBS, pelleted by centrifugation, and resuspended in 300 μL of PBS supplemented with 1% FBS to prevent cell clumping. Intracellular fluorescence levels were measured using a BD LSR flow cytometer (BD Biosciences, San Jose, CA). For **4** and **6**, fluorescence was detected at two wavelengths for the two fluorescent products hydrolyzed in the cell: the aminoquinazoline [excitation at 340 nm and emission at 451 nm (blue)] and the dansylated DNA-damaging species [excitation at 340 nm and emission at 525 nm (green)]. To test the transport efficiency of P-gp-proficient cells (MES-SA/DX5) in comparison with the parental MES-SA P-gp-deficient cells, we quantified the fluorescence levels of doxorubicin [excitation at 480 nm and emission at 560−590 nm (red)] and recorded the percentage of doxorubicin-positive P-pg-expressing cells (MES-SA/DX5). FACS results were analyzed with GraphPad Prism software.

Acknowledgment. We thank the National Cancer Institute of Canada (NCIC Grant 018475), Canadian Institutes of Cancer Research (Grant FRN 49440), and Fonds de la Recherche en Santé du Québec doctoral award (M.T.) for financial support. We gratefully acknowledge Nadim K. Saade from the Department of Chemistry, McGill University, for mass spectra.

References

(1) Ramachandra, M.; Ambudkar, S. V.; Chen, D.; Hrycyna, C. A.; Dey, S.; Gottesman, M. M.; Pastan, I. Human P-Glycoprotein Exhibits Reduced Affinity for Substrates during a Catalytic Transition State. *Biochemistry* **1998**, *37*, 5010–5019.
(2) Sharom, F. J. The P-glycoprotein efflux pump: how does it transport drugs? *J. Membr. Biol.* **1997**, *160*, 161–175.
(3) Szakacs, G.; Paterson, J. K.; Ludwig, J. A.; Booth-Genthe, C.; Gottesman, M. M. Targeting multidrug resistance in cancer. *Nat. Rev. Drug Discovery* **2006**, *5*, 219–234.
(4) Longley, D. B.; Johnston, P. G. Molecular mechanisms of drug resistance. *J. Pathol.* **2005**, *205*, 275–292.
(5) Loo, T. W.; Clarke, D. M. Recent progress in understanding the mechanism of P-glycoprotein-mediated drug efflux. *J. Membr. Biol.* **2005**, *206*, 173–185.
(6) Aller, S. G.; Yu, J.; Ward, A.; Weng, Y.; Chittaboina, S.; Zhuo, R.; Harrell, P. M.; Trinh, Y. T.; Zhang, Q.; Urbatsch, I. L.; Chang, G. Structure of P-Glycoprotein Reveals a Molecular Basis for Poly-Specific Drug Binding. *Science* (*Washington, DC, U. S.*) **2009**, *323*, 1718–1722.
(7) Perez, R. P.; Hamilton, T. C.; Ozols, R. F.; Young, R. C. Mechanisms and modulation of resistance to chemotherapy in ovarian cancer. *Cancer* **1993**, *71*, 1571–80.
(8) Turk, D.; Hall, M. D.; Chu, B. F.; Ludwig, J. A.; Fales, H. M.; Gottesman, M. M.; Szakacs, G. Identification of Compounds Selectively Killing Multidrug-Resistant Cancer Cells. *Cancer Res.* **2009**, *69*, 8293–8301.
(9) Brahimi, F.; Matheson, S. L.; Dudouit, F.; McNamee, J. P.; Tari, A. M.; Jean-Claude, B. J. Inhibition of epidermal growth factor receptor-mediated signaling by "Combi-Triazene" BJ2000, a new probe for Combi-Targeting postulates. *J. Pharmacol. Exp. Ther.* **2002**, *303*, 238–246.
(10) Brahimi, F.; Rachid, Z.; McNamee, J. P.; Alaoui-Jamali, M. A.; Tari, A. M.; Jean-Claude, B. J. Mechanism of action of a novel "combi-triazene" engineered to possess a polar functional group on the alkylating moiety: Evidence for enhancement of potency. *Biochem. Pharmacol.* **2005**, *70*, 511–519.
(11) Brahimi, F.; Rachid, Z.; Qiu, Q.; McNamee, J. P.; Li, Y.-J.; Tari, A. M.; Jean-Claude, B. J. Multiple mechanisms of action of ZR2002 in human breast cancer cells: A novel combi-molecule designed to block signaling mediated by the ERB family of oncogenes and to damage genomic DNA. *Int. J. Cancer* **2004**, *112*, 484–491.
(12) Domarkas, J.; Dudouit, F.; Williams, C.; Qiyu, Q.; Banerjee, R.; Brahimi, F.; Jean-Claude, B. J. The Combi-Targeting Concept: Synthesis of Stable Nitrosoureas Designed to Inhibit the Epidermal Growth Factor Receptor (EGFR). *J. Med. Chem.* **2006**, *49*, 3544–3552.
(13) Banerjee, R.; Rachid, Z.; McNamee, J.; Jean-Claude, B. J. Synthesis of a Prodrug Designed To Release Multiple Inhibitors of the Epidermal Growth Factor Receptor Tyrosine Kinase and an Alkylating Agent: A Novel Tumor Targeting Concept. *J. Med. Chem.* **2003**, *46*, 5546–5551.
(14) Rachid, Z.; Brahimi, F.; Katsoulas, A.; Teoh, N.; Jean-Claude, B. J. The Combi-Targeting Concept: Chemical Dissection of the Dual Targeting Properties of a Series of "Combi-Triazenes. *J. Med. Chem.* **2003**, *46*, 4313–4321.
(15) Todorova, M.; Larroque, A.-L.; Dauphin-Pierre, S.; Fang, Y. Q.; Jean-Claude, B. J. Cellular imaging and signaling to AL237, a fluorescent-labeled probe for the combi-targeting approach to tumor targeting. *Mol. Cancer Ther.* **2009**, accepted for publication.
(16) Yip, W. L.; Weyergang, A.; Berg, K.; Tonnesen, H. H.; Selbo, P. K. Targeted delivery and enhanced cytotoxicity of cetuximab-saporin by photochemical internalization in EGFR-positive cancer cells. *Mol. Pharmaceutics* **2007**, *4*, 241–451.
(17) Harker, W. G.; MacKintosh, F. R.; Sikic, B. I. Development and characterization of a human sarcoma cell line, MES-SA, sensitive to multiple drugs. *Cancer Res.* **1983**, *43*, 4943–4950.
(18) Harker, W. G.; Sikic, B. I. Multidrug (pleiotropic) resistance in doxorubicin-selected variants of the human sarcoma cell line MES-SA. *Cancer Res.* **1985**, *45*, 4091–4096.
(19) Koo, J. S.; Choi, W. C.; Rhee, Y. H.; Lee, H. J.; Lee, E. O.; Ahn, K. S.; Bae, H. S.; Ahn, K. S.; Kang, J. M.; Choi, S. U.; Kim, M. O.; Lu, J.; Kim, S. H. Quinoline derivative KB3−1 potentiates paclitaxel induced cytotoxicity and cycle arrest via multidrug resistance reversal in MES-SA/DX5 cancer cells. *Life Sci* **2008**, *83*, 700–708.
(20) Merayo, N.; Rachid, Z.; Qiu, Q.; Brahimi, F.; Jean-Claude, B. J. The combi-targeting concept: Evidence for the formation of a novel inhibitor in vivo. *Anti-Cancer Drugs* **2006**, *17*, 165–171.
(21) Wang, H.; Giuliano, A. E.; Cabot, M. C. Enhanced de novo ceramide generation through activation of serine palmitoyltransferase by the P-glycoprotein antagonist SDZ PSC 833 in breast cancer cells. *Mol. Cancer Ther.* **2002**, *1*, 719–726.
(22) Liem, A. A.; Appleyard, M. V.; O'Neill, M. A.; Hupp, T. R.; Chamberlain, M. P.; Thompson, A. M. Doxorubicin and vinorelbine act independently via p53 expression and p38 activation respectively in breast cancer cell lines. *Br. J. Cancer* **2003**, *88*, 1281–1284.
(23) Panasci, L.; Jean-Claude, B. J.; Vasilescu, D.; Mustafa, A.; Damian, S.; Damian, Z.; Georges, E.; Liu, Z.; Batist, G.; Leyland-Jones, B. Sensitization to doxorubicin resistance in breast cancer cell lines by tamoxifen and megestrol acetate. *Biochem. Pharmacol.* **1996**, *52*, 1097–1102.
(24) Skehan, P.; Storeng, R.; Scudiero, D.; Monks, A.; McMahon, J.; Vistica, D.; Warren, J. T.; Bokesch, H.; Kenney, S.; Boyd, M. R. New colorimetric cytotoxicity assay for anticancer-drug screening. *J. Natl. Cancer Inst.* **1990**, *82*, 1107–1112.

(25) Matheson, S. L.; McNamee, J. P.; Wang, T.; Alaoui-Jamali, M. A.; Tari, A. M.; Jean-Claude, B. J. The combi-targeting concept: Dissection of the binary mechanism of action of the combi-triazene SMA41 in vitro and antitumor activity in vivo. *J. Pharmacol. Exp. Ther.* **2004**, *311*, 1163–1170.
(26) Olive, P. L.; Banath, J. P. The comet assay: A method to measure DNA damage in individual cells. *Nat. Protoc.* **2006**, *1*, 23–29.
(27) McNamee, J. P.; McLean, J. R.; Ferrarotto, C. L.; Bellier, P. V. Comet assay: Rapid processing of multiple samples. *Mutat. Res.* **2000**, *466*, 63–69.